J|A|C|S
A R T I C L E S

Intrinsic Multistate Switching of Gold Clusters through Electrochemical Gating

Tim Albrecht,*,§ Stijn F. L. Mertens,⊥ and J. Ulstrup*

Contribution from the Department of Chemistry, Nano·DTU, Technical University of Denmark, Kemitorvet, Building 207, 2800 Kongens Lyngby, Denmark

Received April 11, 2007; E-mail: t.albrecht@imperial.ac.uk; ju@kemi.dtu.dk

Abstract: The electrochemical behavior of small metal nanoparticles is governed by Coulomb-like charging and equally spaced charge-transfer transitions. Using electrochemical gating at constant bias voltage, we show, for the first time, that individual nanoparticles can be operated as multistate switches in condensed media at room temperature, displaying distinct peak features in the tunneling current. The tunneling conductance increases with particle charge, suggesting that solvent reorganization and dielectric saturation become increasingly important.

Introduction

Monolayer-protected gold nanoparticles (NPs) have attracted major interest in numerous areas of research, ranging from physics to chemistry and biology.[1] Due to their unique electronic properties, their potential importance in molecular or nanoelectronics was recognized early.[2] The electronic structure of small metal NPs with core diameter smaller than about 1 nm resembles the discrete electronic spectra of similar-size molecules, but bulk properties are approached for particles with core diameters already at, say, 3 nm and larger.[3] In the intermediate size regime, metal NPs behave qualitatively differently from both molecules and bulk material. This renders monolayer-protected NPs in this size range particularly interesting as switching and transistor elements in forthcoming molecular electronic circuitry. Electronic charging is governed by capacitive effects, and, to a first approximation, consecutive charge states are equally spaced energetically by $\Delta\epsilon = e^2/C$, where e is the electronic charge and C the capacitance of the particle. Such capacitive charging has been observed for different types and sizes of nanoparticles, in various environments and using different techniques. The latter include low- and room-temperature scanning tunneling microscopy (STM) and spectroscopy (STS) of immobilized NPs in vacuum or air[4−8] and electrochemical methods applied to both solute NPs and NP layers on noble metal substrate electrodes.[9−14]

First et al. investigated sequential charging of a Au_{146} NP quite similar to the design in the present report and compared charging energies from differential pulse voltammetry (DPV) in solution at room temperature with *ex situ* (i.e., in air or vacuum) STM current/bias voltage relations at 83 K.[7] The peak spacing in DPV was found to decrease with increasing charge on the particle. At potentials close to the potential of zero charge (pzc), however, the energy spacing between subsequent charge states was very similar for the two methods. Over the bias range investigated by STM, the peak spacing remained constant. The decreasing peak spacing observed by electrochemistry was suggested to be due to a change in cluster capacitance or counterion effects for the more highly charged states.
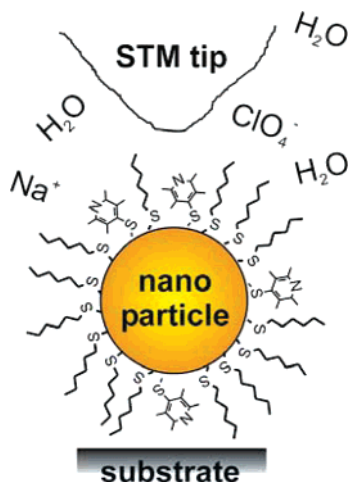
Electrochemical environments offer, further, a unique feature compared to experiments in air or vacuum ("*ex situ*"), namely the notion of full potential control. In electrochemical STM, for example, the potentials of both tip and substrate electrodes, E_t and E_s, are independently controlled with respect to a common reference electrode. The electrochemical potential of the latter is given by its chemical composition, e.g., Ag/AgCl/Cl⁻, and remains constant. Two distinct tunneling spectroscopic tools therefore emerge: tunneling current I_t/V_{bias} spectroscopy at constant $E_{s/t}$ ($V_{bias} = E_t − E_s$), and tunneling current $I_t/E_{s/t}$ spectroscopy at constant V_{bias}. The latter is sometimes referred to as tunneling current/overpotential spectroscopy, where the

§ Present address: Department of Chemistry, Imperial College London, South Kensington Campus, London SW7 2AZ, UK.
⊥ Present address: Institute of Bio- and Nanosystems 3, Research Center Juelich, 52425 Juelich, Germany.

(1) Daniel, M.-C.; Astruc, D. *Chem. Rev.* **2004**, *104*, 293−346.
(2) Schmid, G.; Simon, U. *Chem. Commun.* **2005**, *6*, 697−710 and references therein.
(3) Chen, S.; Ingram, R. S.; Hostetler, M. J.; Pietron, J. J.; Murray, R. W.; Schaaff, T. G.; Khoury, J. T.; Alvarez, M. M.; Whetten, R. L. *Science* **1998**, *280*, 2098−2101.
(4) Andres, R. P.; Bein, T.; Dorogi, M.; Feng, S.; Henderson, J. I.; Kubiak, C. P.; Mahoney, W.; Osifchin, R. G.; Reifenberger, R. *Science* **1996**, *272*, 1323−1325.
(5) Ralph, D. C.; Black, C. T.; Tinkham, M. *Phys. Rev. Lett.* **1995**, *74*, 3241−3244.
(6) Dubois, J. G. A.; Gerritsen, J. W.; Shafranjuk, S. E.; Boon, E. J. G.; Schmid, G.; van Kempen, H. *Europhys. Lett.* **1996**, *33*, 279−284.

(7) Ingram, R. S.; Hostetler, M. J.; Murray, R. W.; Schaaff, T. G.; Khoury, J. T.; Whetten, R. L.; Bigioni, T. P.; Guthrie, D. K.; First, P. N. *J. Am. Chem. Soc.* **1997**, *119*, 9279−9280.
(8) Graf, H.; Vancea, J.; Hoffmann, H. *Appl. Phys. Lett.* **2002**, *80*, 1264−1266.
(9) Chen, S.; Murray, R. W.; Feldberg, S. W. *J. Phys. Chem. B* **1998**, *102*, 9898−9907.
(10) Hicks, J. F.; Miles, D. T.; Murray, R. W. *J. Am. Chem. Soc.* **2002**, *124*, 13322−13328.
(11) Hicks, J. F.; Templeton, A. C.; Chen, S.; Sheran, K. M.; Jasti, R.; Murray, R. W.; Debord, J.; Schaaff, T. G.; Whetten, R. L. *Anal. Chem.* **1999**, *71*, 3703−3711.
(12) Su, B.; Girault, H. H. *J. Phys. Chem. B* **2005**, *109*, 11427−11431.
(13) Su, B.; Zhang, M.; Shao, Y.; Girault, H. H. *J. Phys. Chem. B* **2006**, *110*, 21460−21466.
(14) Quinn, B. M.; Liljeroth, P.; Ruiz, V.; Laaksonen, T.; Kontturi, K. *J. Am. Chem. Soc.* **2003**, *125*, 6644−6645.

Figure 1. Sequential charging events in DPV (red) and $I_t(\eta)$ tunneling spectroscopy (black) at constant $V_{bias} = 0.05$ V ($I_{set}^\circ = 0.05$ nA). Inset: abundance distribution of $I_t(\eta)$ peak positions (binning: 0.03 V). Electrolyte: 0.1 M $KClO_4$ (tunneling spectroscopy) or 0.1 M $NaClO_4$ (DPV).

overpotential $\eta = E_s - E^\circ$, and E° is the equilibrium potential of a redox species. The η dependence of I_t can be utilized to introduce a gating effect with close analogies between electrochemical (*in situ*) STM and conventional electronic transistors, where tip, substrate, and reference electrodes correspond to source, drain, and gate contacts, respectively. This has been exploited to induce transistor function in single redox-active molecules such as Os- or Co-based transition metal complexes.[15−23] Electrochemical gating is not restricted to aqueous environments. We have recently addressed ionic liquids in which an Os complex was brought to exhibit both strong transistor ("amplification") and diode functions with high current amplification and rectification ratios.[24] On the basis of these results, extension toward solid-state ionic conductors as gate media appears feasible and would facilitate electrochemical gating in molecular-scale electronic circuitry.

In the present study, we employ electrochemical gating to probe multiple electronic states of a monolayer-protected gold NP, Au_{145}, with the average composition $Au_{145}(C6S)_{38}(4MP)_{12}$ (C6S, ω-hexylmercaptane; 4MP, 4-mercaptopyridine; Scheme 1). The synthesis and characterization of the NPs, monolayer preparation, and experimental procedures are detailed in the Materials and Methods and in the Supporting Information.

Monolayers of Au_{145} on single-crystal Pt(111) electrodes were first characterized by differential pulse voltammetry (DPV; Figure 1, red curve). Sequential charging events are clearly visible. with an average peak spacing ΔV of 0.148 V or, by $C = e/\Delta V$, a capacitance per NP of 1.08 aF (cf. Figure 2, closed circles). This result is very close to previous data reported by
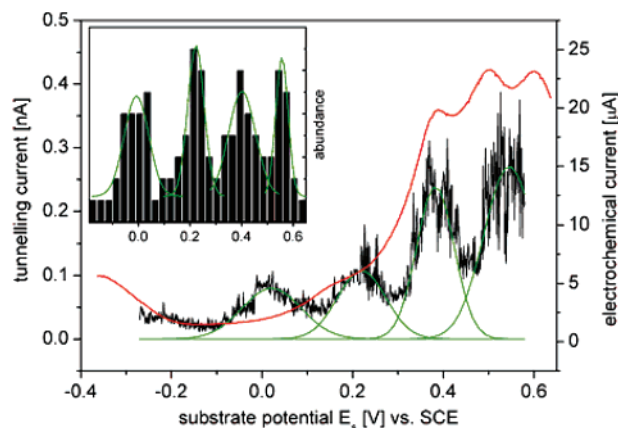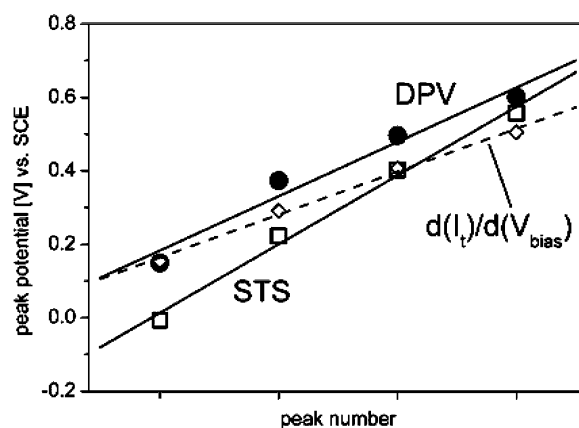
Figure 2. Peak positions of DPV (●), $I_t(\eta)$ ("STS", □), and $d(I_t)/d(V_{bias})$ data (◇), including linear fits. Note that the peak potential for the $d(I_t)/d(V_{bias})$ data refers to E_t, measured at constant E_s, and not to E_s as for the other two. Further details are given in the text.

Chen and Pei, who investigated, *inter alia*, the anion effect on NP charging for Au_{145} with various protecting monolayers.[25,26] We also observe the electrochemical "rectification effect" described by these authors, i.e., more intense charging signals positive of the pzc at around -0.15 V vs saturated calomel electrode (SCE), ascribed to the incorporation of hydrophobic anions at positive substrate potentials. The charging peaks are much less intense at potentials negative of the pzc. We therefore focus on the clearly resolved signals at positive potentials. The electrochemical data thus support the target design of the NP, in agreement with STM and TEM imaging data (Supporting Information).

The charging steps can also be resolved in $I_t(\eta)$ spectroscopy at constant V_{bias}. Figure 1 depicts an example of an $I_t(\eta)$ spectrum (black curve) with clearly resolved tunneling current peaks (green lines show Gaussian fits). Their position and intensity vary somewhat from scan to scan, as the STM tip slowly drifts over the substrate surface. This would create slightly different microenvironments and tunneling conditions for each scan. The abundance distribution of peak positions, however, clearly shows that the peaks are not randomly

(15) Albrecht, T.; Moth-Poulsen, K.; Christensen, J. B.; Guckian, A.; Bjørnholm, T.; Vos, J. G.; Ulstrup, J. *Faraday Discuss.* **2006**, *131*, 265−279.
(16) Albrecht, T.; Guckian, A.; Ulstrup, J.; Vos, J. G. *Nano Lett.* **2005**, *5*, 1451−1455.
(17) Albrecht, T.; Guckian, A.; Kuznetsov, A. M.; Vos, J. G.; Ulstrup, J. *J. Am. Chem. Soc.* **2006**, *128*, 17132−17138.
(18) Tao, N. J. *Phys. Rev. Lett.* **1996**, *76*, 4066−4069.
(19) Xiao, X.; Brune, D.; He, J.; Lindsay, S.; Gorman, C. B.; Tao, N. J. *Chem. Phys.* **2006**, *326*, 138−143.
(20) Xu, B.; Xiao, X.; Yang, X.; Zang, L.; Tao, N. J. *J. Am. Chem. Soc.* **2005**, *127*, 2386−2387.
(21) Chen, F.; He, J.; Nuckolls, C.; Roberts, T.; Klare, J. E.; Lindsay, S. *Nano Lett.* **2005**, *5*, 503−506.
(22) Li, Z.; Han, B.; Meszaros, G.; Pobelov, I.; Wandlowski, T.; Blaszczyk, A.; Mayor, M. *Faraday Discuss.* **2006**, *131*, 121−143.
(23) Li, Z.; Pobelov, I.; Han, B.; Wandlowski, T.; Blaszczyk, A.; Mayor, M. *Nanotechnology* **2007**, *18*, 044018.
(24) Albrecht, T.; Moth-Poulsen, K.; Christensen, J. B.; Hjelm, J.; Bjørnholm, T.; Ulstrup, J. *J. Am. Chem. Soc.* **2006**, *128*, 6574−6575.

(25) Chen, S.; Pei, R. *J. Am. Chem. Soc.* **2001**, *123*, 10607−10615.
(26) Chen, S. *J. Am. Chem. Soc.* **2000**, *122*, 7420−7421.

distributed but accumulate at certain potentials (Figure 1, inset). The peak positions are summarized in Figure 2.

The tunneling current peaks appear in the same potential region as in the DPV experiments. This suggests strongly that they originate from the same effect, *viz.* sequential charging of the NP as the overpotential is increased. The tunneling current is then mediated by each individual charge state. The peak spacing ΔV is, however, larger than in the electrochemical experiments, at 187 mV/peak (vs 148 mV/peak in DPV). Using again $C = e/\Delta V$, this yields a capacitance per particle of 0.86 aF, which is about 20% smaller than the value obtained from DPV.

Murray et al. found that the diffuse layer capacitance contributed about 20% to the total capacitance for a very similar system, hexanethiolate-protected Au_{140} NP in solution (DPV in CH_2Cl_2/Bu_4NClO_4).[27] It could therefore be argued that the observed difference between DPV and $I_t(\eta)$ data in our case is due to changes in the contribution of diffuse layer capacitance. The presence of the STM tip may account for such an effect by replacing part of the solvent around the NP. We will show in the following, however, that another factor can also affect the peak spacing in electrochemical tunneling spectroscopy, namely the potential drop parameter ξ that couples E_s to the local potential at the NP site.

A tunneling current formalism for two-step electron (or hole) transfer via a single molecular redox level has been reported.[28] We extend this model and adapt it to the present case, taking into account the presence of Coulomb charge states. A detailed theoretical treatment of the electrode/nanoparticle/electrode junction in electrochemical environments is beyond the scope of the present article and will be reported elsewhere.

With the separation between adjacent charge states being small compared to that in typical redox molecules, we introduce the two-step tunneling current form in eq 1, valid for small bias voltages, i.e., $|eV_{bias}| < \lambda$ (where λ is the reorganization free energy, cf. below). We take the adiabatic limit of strong electronic interaction between the particle and the enclosing electrodes.

$$i_t^{adiab} = 2ne \sum_j \left[\frac{k_{part,substr}^{el}(j)\, k_{tip,part}^{el}(j)}{k_{part,substr}^{el}(j) + k_{tip,part}^{el}(j)} + \frac{k_{part,substr}^{hole}(j)\, k_{tip,part}^{hole}(j)}{k_{part,substr}^{hole}(j) + k_{tip,part}^{hole}(j)} \right] \quad (1)$$

This form emphasizes that *electron transfer*, i.e., temporary particle state change by excess *negative* charges ("electrons"), and *hole transfer*, i.e., temporary changes by excess *positive* charges ("holes"), are the two tunneling current mechanisms. Essentially this refers to different orders in the substrate/particle and particle/tip electron-transfer steps. Electron transfer, in the sense noted, would dominate at negative and hole transfer at positive substrate overpotentials. The factor n is the number of electrons/holes transferred in a single *in situ* STM charge-transfer event. n is proportional formally to the electronic

transmission coefficients between the nanoparticle and the respective electrodes, κ, the electronic level density on the electrodes, ρ, and V_{bias}.[28] Multiple redox transitions are indicated by the integer j (= $-\infty$, ..., -2, -1, 0, for electron transfer and 0, 1, 2, ..., ∞ for hole transfer).

The following specific rate constant expressions apply to the two ET steps, between substrate and particle, and between particle and tip, respectively, and accommodate both electron and hole transfer in the sense noted:

$$k_{part,substr}^{el}(j) = \frac{\omega_{eff}}{2\pi} \exp\left[-\frac{[\lambda + e\xi\eta - (j - 1/2)(e^2/C) - e\gamma V_{bias}]^2}{4\lambda k_B T} \right] \quad (2)$$

$$k_{tip,part}^{el}(j) = \frac{\omega_{eff}}{2\pi} \exp\left[-\frac{[\lambda - e\xi\eta + (j + 1/2)(e^2/C) - e(1 - \gamma)V_{bias}]^2}{4\lambda k_B T} \right] \quad (3)$$

where λ is the environmental nuclear reorganization free energy, η the overpotential of the substrate electrode relative to the 0/+1 redox transition, V_{bias} the tip/substrate bias ($E_t - E_s$), C the capacitance of the nanoparticle, and ω_{eff} the effective vibrational frequency of all the nuclear modes reorganized. ξ and γ are parametric representations of the fractions of the substrate-solution potential drop and the bias voltage, respectively, at the site of the particle. Negative and positive j thus represent electron and hole transfer, respectively, both in principle at either negative or positive overpotentials.

Equations 2 and 3 prompt some observations and reservations:

(a) We maintain presently the view of solvent activation and relaxation as crucial elements of the charge-transfer process in combination with evenly spaced energy levels. Disregarding contributions from the electronic contacts, the broadening follows roughly $\Delta \approx 2(\lambda k_B T)^{1/2} < e^2/\xi C$. The peaks would become congested when the opposite inequality applies. This pattern resembles vibrational fine structure in electronic spectroscopy.

(b) Equations 2 and 3 apply when the bias voltage is *small*. This condition accords with $\gamma|eV_{bias}| < \lambda - |e\eta|$ in tunneling spectroscopy of molecules. The additional condition $\gamma|eV_{bias}| < e^2/\xi C$ must also apply in the present case. Each peak in the overpotential correlation is replaced by a steplike feature when the opposite condition applies.[29]

(c) An alternative approach would be to frame the data by a model in which solvent activation is disregarded, while solvent relaxation can be either maintained or also disregarded. Such a view can be based on the Breit–Wigner formalism, here equivalent to superexchange through a succession of particle Coulomb levels.[30] The current–overpotential relation would then give a succession of rectangular "pulses" with a "pulse" width of approximately $\gamma|eV_{bias}|$, broadened and smoothed by the electronic contacts to the enclosing electrodes. This view has been used recently to address both electronic transitions at cryogenic temperatures[29] and tunneling spectroscopic patterns of a viologen-based molecule in an electrochemically controlled *in situ* STM contact.[31] We shall not pursue this view further in the present report.

(27) Guo, R.; Georganopoulo, D.; Feldberg, S. W.; Donkers, R.; Murray, R. W. *Anal. Chem.* **2005**, *77*, 2662–2669.
(28) Zhang, J.; Chi, Q.; Kuznetsov, A. M.; Hansen, A. G.; Wackerbarth, H.; Christensen, H. E. M.; Andersen, J. E. T.; Ulstrup, J. *J. Phys. Chem. B* **2002**, *106*, 1131–1152.

(29) Kuznetsov, A. M.; Ulstrup, J. *J. Electroanal. Chem.* **2004**, *564*, 209–222.
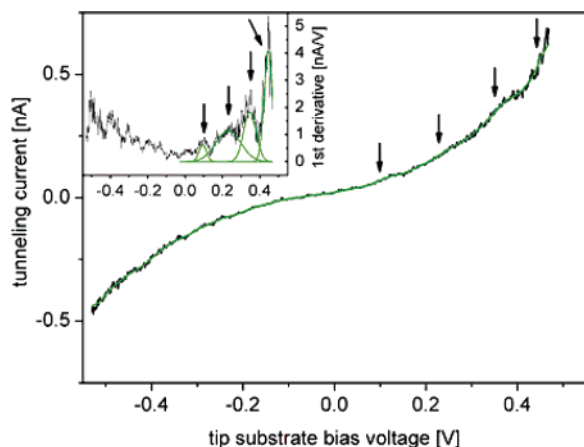(30) Datta, S. *Electronic Transport in Mesoscopic Systems*; Cambridge University Press: Cambridge, 1995.

Figure 3. $I_t(V_{bias})$ spectroscopy with $E_s = +0.03$ V vs SCE (constant), averaged experimental data (10 curves, black), and smoothed curve (green); arrows indicate inflection points. Inset: first derivative of the smoothed curve, with arrows indicating Gaussian peak positions (green).

Figure 4. Tunneling current peak intensity for the four charging steps depicted in Figure 1. Despite a somewhat wide distribution of peak currents, a notable overall increase is observed with increasing charge state. See text for further details.

(d) The current/bias voltage dependence also gives discrete features, separated roughly by $e^2/\gamma C$, but now with the character of successive steps, or inflection points, rather than a succession of peaks. The formalism, however, needs extension to limits of large bias voltages to incorporate these features explicitly, as reported in refs 28 and 32.

The observed overpotential dependence of the tunneling current shows a progression of evenly spaced peaks. By eqs 2 and 3, the peak separation is $e^2/\xi C$. Apart from the NP capacitance C, the model predicts an additional contribution to the peak spacing in $I_t(\eta)$ spectroscopy, namely the parameter ξ. With $0 \leq \xi \leq 1$, the peak spacing can be larger than observed in electrochemistry. Assuming that the NP capacitance is the same for DPV and $I_t(\eta)$ spectroscopy, $C_{DPV} = 1.08$ aF/particle, and ΔV from $I_t(\eta)$ spectroscopy (0.19 V), we obtain $\xi = 0.8$. This would imply that the local potential at the nanoparticle responds strongly to changes of E_s.[33]

Furthermore, the model predicts distinct charging events as steplike features in $I_t(V_{bias})$ spectroscopy, this time with the peak spacing ΔV modulated by γ ($\Delta V = e/\gamma C$). We therefore recorded $I_t(V_{bias})$ spectra, as exemplified in Figure 3. In these experiments, the substrate potential E_s was kept constant at $+0.03$ V vs SCE, while the tip potential E_t was swept from -0.5 to $+0.5$ V. The feedback loop was switched off during the potential sweep, and the tip/substrate distance was defined by the initial setpoint current $I_{set}^\circ = 0.5$ nA.

Steplike tunneling current features seem to be present indeed, even though their exact location in terms of potential is difficult to determine precisely. After smoothing the averaged experimental $I_t(V_{bias})$ curve, we determined the position of the step feature from the first derivative (inset of Figure 3). The results obtained in this way are plotted in Figure 2 (open diamonds). The peak separation of 117 mV is smaller than the two values from DPV and $I_t(\eta)$ spectroscopy and would give a capacitance of 1.37 aF/particle for $\gamma = 1$. While this is larger than the values
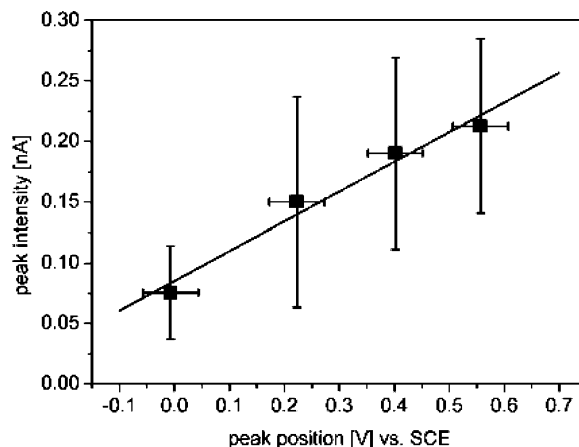
from both DPV and $I_t(\eta)$ spectroscopy, the result requires further consideration.

First, it should be noted that the potential settings were different from those used in the $I_t(\eta)$ tunneling experiments displayed in Figure 1. $I_t(\eta)$ spectroscopy was recorded at $V_{bias} = 0.05$ V and with the substrate potential sweep starting at $E_{s,i} = -0.27$ V vs SCE. In comparison, $I_{set}^\circ = 0.5$ nA and $V_{bias} = -0.5$ V in $I_t(V_{bias})$ spectroscopy (constant $E_s = +0.03$ V vs SCE). Each parameter affects the conductance of the tunneling junction.

Second, due to different V_{bias} and I_{set}° settings in the two cases when the feedback loop is switched off, the tip/substrate distance is also different. This has been shown to affect the overall conductance of the tunneling junction.[17]

A similar behavior was observed by First et al., who compared solution DPV with *ex situ* tunneling spectroscopy data for a hexanethiol-protected Au_{146} NP.[7] They detected sequential charging events in both cases, with very similar potential spacings between different charge states close to the pzc. At substrate potentials further from the pzc, however, the DPV peak decreased from about 400 mV to 200 mV. The authors did not offer an explicit explanation for their observation, but the strong electric fields corresponding to $E_s \gg$ pzc may be similar to the situation in the electric double layer, in particular at high V_{bias}. It still remains unclear why strong electric fields would cause a decrease in peak spacing, and further work is required to answer this question.

From the first derivative of the $I_t(V_{bias})$ curve (Figure 3, inset), we obtained conductance values of 0.7, 1.2, 2.0, and 4.2 nS for the four charging steps, each at different V_{bias}. This compares well with the $I_t(\eta)$ spectroscopy data (cf. below).

Tunneling current−distance spectroscopy ($I_t(z)$) supports the conductance data. In about 10−20% of all $I_t(z)$ traces, we observed characteristic "jumps" in the tunneling current at around 0.2−0.3 nA ($V_{bias} = 0.1$ V). All other curves were either excessively noisy or featureless.[19] The current steps could be interpreted as physical contact between the STM tip and the NP, even though the exact nature of the underlying process is not clear in the present case. Following this interpretation, the $I_t(z)$ curves further suggest that the tip/NP gap is presumably small under the conditions applied in $I_t(\eta)$ spectroscopy ($I_{set}^\circ = 0.05$ nA, $V_{bias} = 0.05$ V), because the current steps occurred

(31) Haiss, W.; Albrecht, T.; van Zalinge, H.; Higgins, S. J.; Bethell, D.; Höbenreich, H.; Schiffrin, D. J.; Nichols, R. J.; Kuznetsov, A. M.; Zhang, J.; Chi, Q.; Ulstrup, J. *J. Phys. Chem. B* **2007**, *111*, 6703−6712.
(32) Kornyshev, A. A.; Kuznetsov, A. M.; Ulstrup, J. *ChemPhysChem* **2005**, *6*, 583−586.
(33) Kuznetsov, A. M.; Ulstrup, J. *J. Phys. Chem. A* **2000**, *104*, 11531−11540; **2001**, *105*, 7494 (erratum).

at $I_t \approx 0.08$ nA. We note, however, that Wandlowski and Nagy observed similar features on a clean gold surface in electrolyte solution, which they ascribed to substructure of the electric double layer.[34] We refer to the Supporting Information for further details on the $I_t(z)$ spectroscopy.

In order to obtain the conductance for each individual charge state, we analyzed the peak current distribution around the average peak potentials $E_{p,j}$ (binning $\pm$ 0.05 V). The average peak currents within these intervals, which correspond to conductance values of 1.7, 2.8, 3.7, and 4.4 nS for the four charging peaks (from left to right), are plotted versus the average peak potential $E_{p,j}$ in Figure 4. The vertical error bars represent the standard deviation $\pm \sigma$; the horizontal ones correspond to ± 0.05 V.

Such conductance values are typical of small organic molecules and suggest that a significant part of the tunneling resistance stems from the protective layer around the NP.[35−38] Similar conclusions have been based on kinetic data from monolayer electrochemistry, lateral conductance measurements on Langmuir−Blodgett films, and experiments on solid-state films of ligand-protected Au_{38}, Au_{140}, Au_{309}, and Au_{976} particles.[39−41] The quantitative contribution of a single bifunctional pyridyl ligand in the NP shell to the total junction conductance, however, presently remains unclear and requires further studies.

The apparent increase in junction conductance with increasing η is an intriguing feature, considering that the tip/substrate distance and V_{bias} were kept constant during each measurement. Despite some scatter in the data, a regression analysis yields an increase of about 50 pA per charge state. The reason for this effect is unlikely to be an increase in electronic coupling. With increasing positive NP charge, the electronic density is rather expected to contract, thus lowering the electronic overlap and decreasing the tunneling peak currents.

On the basis of the model introduced, we suggest an alternative scenario that can qualitatively explain the conductance data. This view rests on the observation that high particle charges j induce strong electric fields in the immediate surroundings, in analogy to highly charged metal ions in solution. This results in a significant degree of structural organization of the solvent molecules, long known as "dielectric saturation".[42−44] The solvent response to a change in charge is then smaller, and the solvent component of the total reorganization free energy λ_{sol} decreases. As a consequence, the ET rate constants for the two tunneling steps increase with increasing particle charge j (cf. eqs 2 and 3), which leads to higher tunneling peak currents
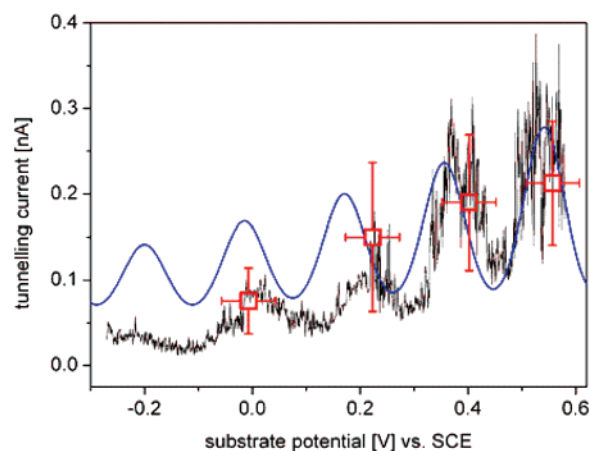
(34) Nagy, G.; Wandlowski, T. *Langmuir* **2003**, *19*, 10271−10280.
(35) Salomon, A.; Cahen, D.; Lindsay, S.; Tomfohr, J.; Engelkes, V. B.; Frisbie, C. D. *Adv. Mater.* **2003**, *15*, 1881−1890.
(36) Gittins, D. I.; Bethell, D.; Schiffrin, D. J.; Nichols, R. J. *Nature* **2000**, *408*, 67−69.
(37) Hipps, K. W. *Science* **2001**, *294*, 536−537.
(38) Zhou, Q.; Li, X.; Fan, Q.; Zhang, X.; Zheng, J. *Angew. Chem., Int. Ed.* **2006**, *45*, 3970−3973.
(39) Choi, J.-P.; Murray, R. W. *J. Am. Chem. Soc.* **2006**, *128*, 10496−10502.
(40) Wuelfing, W. P.; Murray, R. W. *J. Phys. Chem. B* **2002**, *106*, 3139−3145.
(41) Wuelfing, W. P.; Green, S. J.; Pietron, J. J.; Cliffel, D. E.; Murray, R. W. *J. Am. Chem. Soc.* **2000**, *122*, 11465−11472.
(42) Booth, F. *J. Chem. Phys.* **1951**, *19*, 391−394; *19*, 1327 (erratum); *19*, 1615 (erratum).
(43) Liszi, J.; Ruff, I. In *The Chemical Physics of Solvation*; Dogonadze, R. R., Kalman, E., Kornyshev, A. A., Ulstrup, J., Eds.; Elsevier: Amsterdam, 1985; pp 119−141.
(44) Karlström, G. *J. Phys. Chem. B* **2002**, *106*, 5302−5311.
(45) Gosavi, S.; Marcus, R. A. *J. Phys. Chem. B* **2000**, *104*, 2067−2072.

Figure 5. Simulation based on a modified eq 1 with $\lambda(j) = \lambda(j=0) - j\Delta\lambda$ and comparison with an experimental $I_t(\eta)$ trace from Figure 1 (black curve). Red squares, experimental average peak position and peak current (from statistical analysis); blue curve, simulated $I_t(\eta)$ curve. $\lambda(j=0) = 0.2$ eV, $\Delta\lambda = 0.02$ eV/charge state; $C = 1.08$ aF, $\xi = 0.8$; $\gamma = 0.5$; $V_{bias} = 0.05$ V; $\kappa_L = \kappa_R = 1$; $\omega_{eff} = 1 \times 10^{12}$ s^{-1}; $\rho = 2.20$ eV^{-1} (for Pt).[45] The potential axis for the simulated curve was shifted by -0.2 V.

and junction conductance $G(j)$. For simple redox systems in solution, this effect was found to be important for $j \geq 2$.[42−44] On the other hand, in our $I_t(\eta)$ spectroscopy experiments, j rises from 0 to 4 as the overpotential η is increased. It is therefore likely that dielectric saturation is important here as well. Simulations based on eq 1 show that the change in λ required to reproduce the increase in peak current of 50 pA per charge state is not large. Figure 5 illustrates this for a set of parameters, including a j-dependent λ, and compares them once again with the experimental $I_t(\eta)$ data in Figure 1. More systematic simulations showing the effect of the most important parameters in eq 1 on the $I_t(\eta)$ spectrum are described in the Supporting Information.

This hypothesis is attractive, as it explains the qualitative trend in the junction conductance obtained from $I_t(\eta)$ spectroscopy at constant V_{bias}. It is supported by evidence elsewhere that shows that dielectric saturation and charge dependence of the reorganization free energy λ are indeed important for highly charged systems in dielectric media.[42−44]

Dielectric saturation should also affect the particle capacitance and thus the peak spacing observed in $I_t(\eta)$ spectroscopy. Neglecting possible other effects, such as ion pairing, we would expect dielectric saturation to lead to a decrease in the local dielectric constant ϵ_r and in C, and thus to an increase in ΔV. As no large variations of ΔV in the potential range studied were observed, we took the NP capacitance C as constant in the simulations. We thus also disregard such effects on the charge-transfer rate constants k.

Our previous studies on inorganic transition metal complexes of approximately the same size as the 1.6 nm Au-NPs presently in focus showed that electrochemical gating can be used to induce characteristics similar to those of switching, amplification, and rectification at the level of the single molecule.[15−17,24] Even though they are of similar sizes, the electronic structures of the Au-NPs are, however, fundamentally different from molecular electronic structures. The highly conspicuous feature of successive capacitive charging is reminiscent of successive electronic charging of molecules through several oxidation states. At the same time, the different character of the successive

NP charging processes and the much closer and equidistant level spacing offer new perspectives on multistate electronic switching in condensed matter environments at room temperature. This could hardly be offered by "proper" molecules, which usually display much larger redox level spacings.

Our present findings further incorporate new elements of condensed matter charge-transfer theory that explore the complex interplay between reorganization free energy and Coulomb charging. With a view on potential nanoscale electronic devices and components that operate at room temperature and in condensed matter environments, the aqueous medium used in the present study may be fraught with disadvantages. The aqueous medium can, however, be replaced by other nonvolatile condensed media such as ionic liquids and, perhaps, be extended to inorganic solid-state ionic conductors or organic conducting polymers.[46,47]

Materials and Methods

All chemicals were of the highest commercially available purity and used as received. *n*-Hexanethiolate-protected gold nanoparticles were synthesized using the Brust−Schiffrin protocol, with modifications described by Murray and co-workers.[11,48] In short, $[AuCl_4]^-$ was phase-transferred in a water−toluene system using tetra-*n*-octylammonium bromide. After addition of *n*-hexanethiol in a 3:1 molar thiol:gold ratio, $[AuCl_4]^-$ was reduced using sodium borohydride in 10-fold excess at 0 °C. The reduction was allowed to proceed for 45 min, followed by separation of the liquid phases and rotary evaporation of the organic fraction at low temperature (<30 °C). A nanoparticle fraction, for our purpose sufficiently monodisperse, was isolated by ethanol extraction of the crude reaction product. This procedure has been demonstrated to yield primarily particles with Au_{145} cores.[11] After filtration (PTFE membrane 0.2 μm) of the ethanol-soluble cluster fraction, the solvent was rotary-evaporated without heating, and reaction byproducts were removed by copious rinsing with acetonitrile (MeCN).

In order to facilitate nanoparticle immobilization on Pt(111) single-crystal electrode surfaces, 4-mercaptopyridine (4MP) was introduced in the protective monolayer of the nanoparticles by place-exchange.[49] To this end, 9.8 mg of C6S-protected Au_{145} was co-dissolved with 0.5 mg of 4,4′-dithiodipyridine (i.e., the disulfide of 4MP) in 5 cm^3 of toluene and stirred for 48 h. The cluster material was subsequently precipitated by addition of MeCN and filtered over a PTFE membrane. The solid was copiously rinsed with MeCN to remove exchanged *n*-hexanethiol and excess 4MP. Assuming a 1:1 correspondence between outgoing and incoming ligands and full equilibration of the ligand shell with the free ligands in solution, and neglecting steric hindrance for the incoming ligands, the composition of the final product can be estimated as $Au_{145}(C6S)_{38}(4MP)_{12}$. The composition of the ligand shell was not determined analytically, as this was not considered essential for our purpose. Intermediate and final cluster products were characterized using transmission electron microscopy (TEM, see Supporting Information), yielding an average core diameter for the final mixed-monolayer-protected cluster of 1.69 ± 0.29 nm, which is supportive of the above formula.

Supporting Information Available: *In situ* STM image of the Pt surface fully covered with Au_{145}; TEM pictures including size analysis for Au_{145}; features of the theoretical model and simulation results; experimental results from $I_t(z)$ spectroscopy. This material is available free of charge via the Internet at http://pubs.acs.org.

JA072517H

(46) Schuster, M. F. H.; Meyer, W. H. *Annu. Rev. Mater. Res.* **2003**, *85*, 233−261.
(47) Knauth, P.; Tuller, H. L. *J. Am. Ceram. Soc.* **2002**, *85*, 1654−1680.
(48) Brust, M.; Walker, M.; Bethell, D.; Schiffrin, D. J.; Whyman, R. *J. Chem. Soc., Chem. Commun.* **1994**, *7*, 801−802.

(49) Ingram, R. S.; Hostetler, M. J.; Murray, R. W. *J. Am. Chem. Soc.* **1997**, *119*, 9175−9178.